Enhancing Electrocatalytic Synthesis of Glycine with $CuPb_{1ML}$ Electrode Synthesized via Pb UPD

Broersen, P.J.L.; de Groot, T.; Bruggeman, D.F.; Caarls, E.S.; Trindell, J.A.; Anastasiadou, D.; Figueiredo, M.C.; Rothenberg, G.; Garcia, Amanda .C.

DOI
10.1002/cctc.202301370

Publication date
2024

Document Version
Final published version

Published in
ChemCatChem

License
CC BY

ChemCatChem

Research Article
doi.org/10.1002/cctc.202301370

Chemistry Europe
European Chemical Societies Publishing

www.chemcatchem.org

Enhancing Electrocatalytic Synthesis of Glycine with $CuPb_{1ML}$ Electrode Synthesized via Pb UPD

Pim J. L. Broersen,[a] Thijs. de Groot,[a] Didjay F. Bruggeman,[a] Emma S. Caarls,[a] Jamie A. Trindell,[b] Dimitra Anastasiadou,[c] Marta C. Figueiredo,[c] Gadi Rothenberg,[a] and Amanda C. Garcia*[a]

In the field of reductive organic electrosynthesis, the hydrogen evolution reaction (HER) is considered a parasitic reaction that lowers the Faradaic efficiency of the synthesis. Metals with a high overpotential for HER are often used to prevent this. However, this limits the catalytic materials that can be used in these reactions. To expand upon the scope of available electrocatalysts, we prepared a CuPb electrode via underpotential deposition (UPD). We thereby created an electrocatalyst with a single monolayer of Pb, $CuPb_{1ML}$, in which Pb weight loading is only 415 ng cm^{-2}, yet its properties could still effectively inhibit HER. The $CuPb_{1ML}$ electrode was used in the electrosynthesis of glycine from oxalic acid and hydroxylamine. This reaction served as a model for a C–N bond forming reaction in acidic aqueous media. The $CuPb_{1ML}$ electrode was compared against a pure Pb and Cu metal electrode. The $CuPb_{1ML}$ electrode showed a Faradaic efficiency for glycine production of 57%, which was 9-fold higher than Cu and rivaled the Pb electrode. The catalytic activity of $CuPb_{1ML}$ was 211 μmol h^{-1} cm^{-2}, which is higher than both Cu and Pb. The mechanism of the electroreduction was then studied via *in situ* Fourier Transform Infra-Red (FTIR) spectroscopy. These results hinted to an evolution of the electrocatalyst during the electrolysis reaction, which was then studied via Scanning Electron Microscopy (SEM) and X-Ray Photoelectron spectroscopy (XPS). We found that the Pb monolayer restructured during catalysis, forming microparticles that were active in the reaction based on the listed experiments. Pb alloying into the lattice, which can occur during UPD, also lowered the HER, further facilitating glycine synthesis. Thus, our research also shows how Pb UPD impacts the catalytic properties of a metal both through monolayer deposition as well as surface alloying.

Introduction

The energy transition and the electrification of industrial sectors brings both challenges and opportunities. Organic electrosynthesis is the direct application of electrons for chemical transformations and is an interesting approach to chemical synthesis. It is accomplished by allowing redox transformations to be performed through direct interaction with an electrocatalyst.[1] Because it uses fewer stoichiometric chemical redox reagents, the electrochemical method is safer and cheaper than conventional thermochemistry.[2] In recent years, there has been a surge of interest in electrosynthesis reactions that form a C–N bond. Several interesting transformations are possible here, including the synthesis of simple amines, amino acids, and fertilizers such as urea.[3–7] As a result, making C–N bond-containing molecules *via* electrosynthesis is an interesting process for industrial application.

A comparison of literature studies on electrochemical C–N bond formation reveals that they are often synthesized through electroreduction in aqueous media.[8–10] Consequently, the hydrogen evolution reaction (HER) is an unwanted side reaction, as it can lower the overall Faradaic efficiency (FE) of the process.[11] Traditionally, when performing electroreduction in water, proton reduction is avoided by choosing an electrode material with a high HER overpotential.[12] However, this limits the possibility of using metals with interesting electrocatalytic capabilities, as they are often also good catalyst for the HER.[13,14]

Copper electrodes, for example, are interesting since they are effective electrocatalysts both in the CO_2 reduction reaction and in NO_3^- reduction.[15,16] Therefore, it is not surprising that C–N bond forming electroreductive reactions frequently use Cu-based materials.[17–19] The problem with using Cu based catalysts is that Cu can also perform HER, especially when using an acidic electrolyte.[20] In this work, we therefore set out to find a method which allows us to limit the HER of a Cu electrode

[a] P. J. L. Broersen, T. de Groot, Dr. D. F. Bruggeman, E. S. Caarls, Prof. Dr. G. Rothenberg, Prof. Dr. A. C. Garcia
Van't Hoff Institute for Molecular Sciences
University of Amsterdam
Science Park 904, 1098 XH, Amsterdam, The Netherlands
E-mail: a.c.garcia@uva.nl

[b] Dr. J. A. Trindell
Gorlaeus Laboratories
Leiden Institute of Chemistry
Leiden University
P.O. Box 9502, 2300 RA, Leiden, The Netherlands

[c] Dr. D. Anastasiadou, Prof. Dr. M. C. Figueiredo
Department of Chemical Engineering and Chemistry
Eindhoven University of Technology
P.O. Box 513, 5600 MB Eindhoven, The Netherlands

Supporting information for this article is available on the WWW under https://doi.org/10.1002/cctc.202301370

and thereby improve its efficiency in electroreductive C–N bond formation in aqueous acid media.

Our strategy was to deposit a minimum amount of lead (Pb) metal, which has a high overpotential for HER, on a Cu surface. We envisioned this could be achieved by using underpotential deposition (UPD)[21] of Pb. UPD deposits only a single monolayer on the electrode, which we postulated could already significantly impact the catalytic capabilities of the electrode. To test our hypothesis, we chose the electrosynthesis of glycine as a model reaction. Glycine electrosynthesis is performed in acidic aqueous media, which is prone to HER. Glycine itself is a worthy product because it is both a food supplement and an additive for various pharmaceuticals,[22] making it an ideal candidate to test our strategy.

We found that the deposition of a single monolayer of Pb on Cu ($CuPb_{1ML}$) resulted in an efficient electrocatalyst, with high FE for glycine that was comparable to that of a pure Pb electrode. Additionally, the electrocatalytic activity of $CuPb_{1ML}$ was greater than both the pure Cu and Pb metals. Further mechanistic study of the $CuPb_{1ML}$ electrode was performed using *in situ* Fourier Transform Infra-Red spectroscopy (FTIR), as well as surface analysis by Scanning Electron Microscopy and X-Ray Photoelectron spectroscopy (SEM and XPS) to study the electrocatalyst before, during and after reaction. Our results showed that the Pb monolayer on Cu is highly mobile during electrocatalysis, forming Pb microparticles on the surface, revealing the Cu layer underneath. Further interpretation of these results indicates that the inhibition of HER is not only caused through the deposition of the Pb monolayer, but also due to surface alloying of Pb with Cu metal.

Results and Discussion

A Cu electrode with a single lead monolayer was prepared via Pb UPD (herein denoted as $CuPb_{1ML}$).[21] The electrode was then characterized or used as the electrocatalyst in the synthesis of glycine from hydroxylamine and oxalic acid as an electroreductive model reaction.[4]

$CuPb_{1ML}$ electrode preparation and characterization

The principle of UPD hinges on the unusual phenomenon that some heterometallic bonds are stronger than their homometallic analogues.[23] In this specific example, the Cu–Pb bond is stronger than the Pb–Pb bond. Therefore, one can form Cu–Pb bonds by applying a potential on a Cu electrode that is less negative than the thermodynamic potential for Pb reduction/oxidation. By applying this potential in an electrolyte containing Pb ions, Cu–Pb bonds will be formed until a full monolayer coverage of the electrode is reached, thereby synthesizing a $CuPb_{1ML}$ electrode. This principle is further illustrated by a typical CV (Figure 1) where an electropolished Cu electrode is cycled in a 0.2 mM $Pb(ClO_4)_2$ and 10 mM $HClO_4$ solution.[24] Following the scan direction, we see first the UPD deposition event *(i)* at approximately −0.1 V vs. RHE. Subsequently the

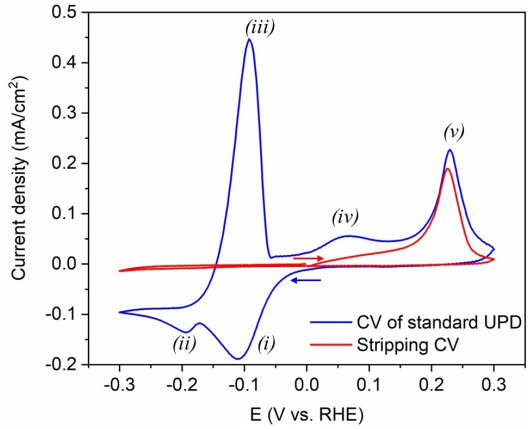

Figure 1. Cyclic voltammogram of a Cu electrode in an aqueous solution containing 0.01 M $HClO_4$ and 0.2 mM $PbClO_4$ (Blue line). Stripping cyclic voltammogram of a freshly prepared $CuPb_{1ML}$ electrode in an aqueous solution containing 0.01 M $HClO_4$ (Red line). Cyclic voltammograms were taken at room temperature with a scan rate of 50 mV s^{-1}. Scan direction indicated in figure.

reduction event at ca. −0.2 V vs. RHE *(ii)* and its associated oxidation *(iii)* at −0.15 V vs. RHE show the thermodynamic redox potential of Pb. In agreement with previous reports using Cu single crystals,[23] the UPD stripping peaks are visible at around 0.05 V vs. RHE *(iv)*, which corresponds to the stripping of Pb from Cu(100) sites, whereas the peak at 0.2 V vs. RHE *(v)* corresponds to the stripping of Pb from Cu(111) sites. After performing the CV, the $CuPb_{1ML}$ electrode was synthesized by applying a potential of −0.1 V vs. RHE for 5 minutes.

The stability of the $CuPb_{1ML}$ electrode was evaluated via CV. Previous research by Vasilic *et al.* showed that the Pb monolayer on a Cu electrode is susceptible to rapid oxidation at open circuit potential, after which the Pb ions are said to dissolve in the electrolyte.[24] However, Brankovic *et al.* showed that a Pb monolayer can remain stable on a Au substrate electrode under inert conditions.[25] Therefore, to verify the stability of our Pb monolayer, we ran three different measurements. First, a stripping CV was performed in a Pb-free solution under inert conditions (Figure 1 –red line, see also detailed description in SI section 3). The CV showed a retention of both the current profile and the area of the UPD stripping peaks, indicating that removing the electrode from the electrolyte does not change the Pb monolayer. We also studied the influence of O_2 on the freshly prepared $CuPb_{1ML}$ electrode using SEM and XPS. SEM images (Figure S1A and S1B) show that after contact with air the electrode remains flat, with no agglomerates, supporting our claim that the Pb monolayer does not restructure upon removal from the electrolyte solution. The XPS data (Figure S1C, S1D and S1E) indicate that Pb is fully oxidized to a native oxide (PbO, with a binding energy (BE) of the Pb $4f_{7/2}$ orbital of 138.3 eV[26]). The Pb content of 1.95 atomic percentage is comparable to other Pb UPD studies.[27] The Pb weight loading was calculated as 415 ng cm^{-2} (Equation S1 in SI), well below the toxicity requirements.[28] Based on our findings, we concluded that Pb UPD is a suitable method for preparing our $CuPb_{1ML}$ electrocatalyst.

Electrochemical measurements

Prior to bulk electrolysis, the $CuPb_{1ML}$ electrode was electrochemically characterized by CV in a blank aqueous 0.1 M H_2SO_4 solution (Figure 2A). Afterwards, its activity was studied in a 0.1 M H_2SO_4 aqueous solution containing 0.25 M oxalic acid and 0.25 M hydroxylamine (Figure 2B). The results for Cu and Pb electrodes are also included for comparison.

In the blank solution, the Pb electrode shows a broad anodic peak (*i*) corresponding to the $Pb/PbSO_4$ redox process at −0.1 V vs. RHE and a smaller cathodic peak (*ii*) at approximately −0.35 V vs. RHE that corresponds to the irreversible reductive desorption of the $PbSO_4$ layer.[29–31] A slight increase in current density is observed at high negative potential (~ −1.0 V vs. RHE) likely due to HER.[32] Conversely, both the Cu and $CuPb_{1ML}$ electrodes showed an increase in current density at potentials more negative than −0.4 V vs. RHE, which was considered to be caused by HER.[33] Surprisingly, even with a Pb monolayer on the Cu surface, hydrogen evolution is not completely suppressed. We only observe a slight shift of approximately 0.1 V towards more negative onset potential when compared to a pure Cu electrode.

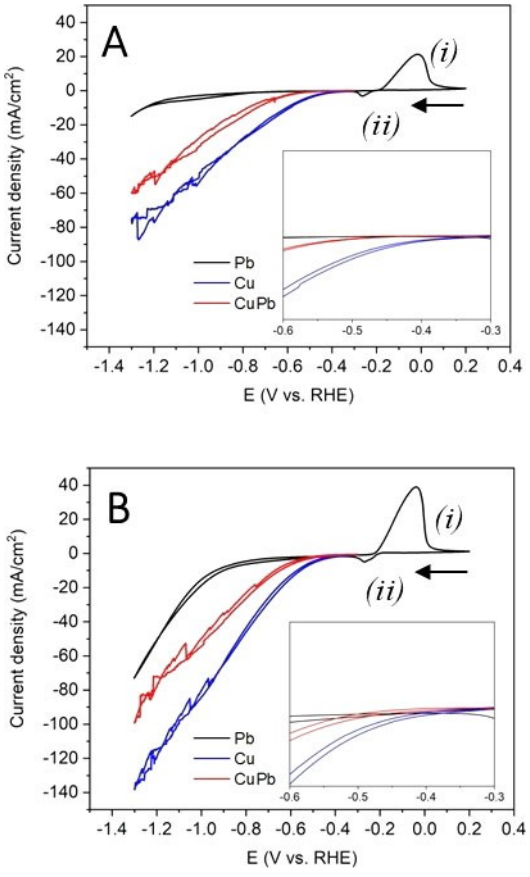

Figure 2. Cyclic voltammograms of Pb (black line), Cu (blue line), and $CuPb_{1ML}$ (red line) working electrodes in 0.1 M H_2SO_4 (aq) in A) a blank electrolyte solution and B) in the presence of 0.25 M oxalic acid and 0.25 M hydroxylamine. Measured at room temperature with a scan rate of 50 mV s^{-1}. Scan direction indicated in figure.

Upon adding 0.25 M oxalic acid and 0.25 M hydroxylamine (Figure 2B), all electrodes showed an increase in current density, likely due to the electrochemical reduction of the substrate (oxalic acid).[3] On the Pb electrode, the reductive process occurs at potentials lower than −0.8 V vs. RHE, whereas on both Cu and $CuPb_{1ML}$ electrodes, as there is no significant shift in potential, we surmise that hydrogen evolution and electroreductive amination are competing.

Electrochemical reductive amination of oxalic acid

The electrocatalytic activity of the $CuPb_{1ML}$ electrode was studied for the electroreductive amination of oxalic acid with hydroxylamine to glycine as a model reaction. Chronoamperometry measurements were performed at various potentials ranging from −0.7 V and −1.3 V vs. RHE for 4 hours and the FE and yields are shown in Figure 3A and B, respectively. Previous work using an amalgamated Cu electrode (e.g. Hg alloyed) showed an inverse correlation between the FE and the applied potential.[3] Conversely, our results show that at potentials more negative than −1.0 V vs. RHE, the FE towards glycine increases considerably (Figure 3A). The maximum FE of glycine of 57% was reached at −1.3 V vs. RHE corresponding to a glycine yield of 48% with a total conversion of oxalic acid of 76% (Figure 3B). These findings demonstrate that the amination reaction outperforms the competitive HER in this potential range.

The carbon balance is also significantly lower (87%), indicating some unidentified products. In another study, Xian *et al.* show that the oxime intermediate can decarboxylate in the electrosynthesis of amino acids, producing a nitrile product.[34] In our system, this nitrile would be hydrogen cyanide (HCN), which we would not detect with our analysis method. Therefore, to minimize the risk of toxic HCN formation and to maintain the carbon balance, we did not perform chronoamperometry at potentials more negative than −1.3 V vs. RHE.

To examine the impact of the Pb monolayer on Cu on the electroreductive amination performance, we also carried out this reaction using the pure metal electrodes Pb and Cu at the optimized potential of the $CuPb_{1ML}$ electrode at −1.3 V vs. RHE (Figure 4). Figure 4A shows the FE of the various products after 4 hours of electrolysis. The $CuPb_{1ML}$ electrodes outperform Cu in terms of FE% for glycine (57% and 9%, respectively), while the FE% of Pb electrode was slightly higher (60%). However, the total glycine formation rate (Figure 4B) was higher on $CuPb_{1ML}$ electrode (211 μmol h^{-1} cm^{-2}) than on either Cu (139 μmol h^{-1} cm^{-2}) or Pb (114 μmol h^{-1} cm^{-2}). This indicates that the $CuPb_{1ML}$ material is an efficient electrocatalyst for the electro-amination reaction, as it produces glycine with high yield and selectivity. The increase in both FE and total glycine formation rate supports the concept that the presence of just one Pb monolayer on Cu is enough to significantly inhibit HER. Finally, the stability of the $CuPb_{1ML}$ electrode was tested over 48 h at −1.3 V vs. RHE. Over this period, the FE towards glycine was reduced to 30%. This decline in FE shows that the $CuPb_{1ML}$ electrode has limited stability over long reaction period, never-

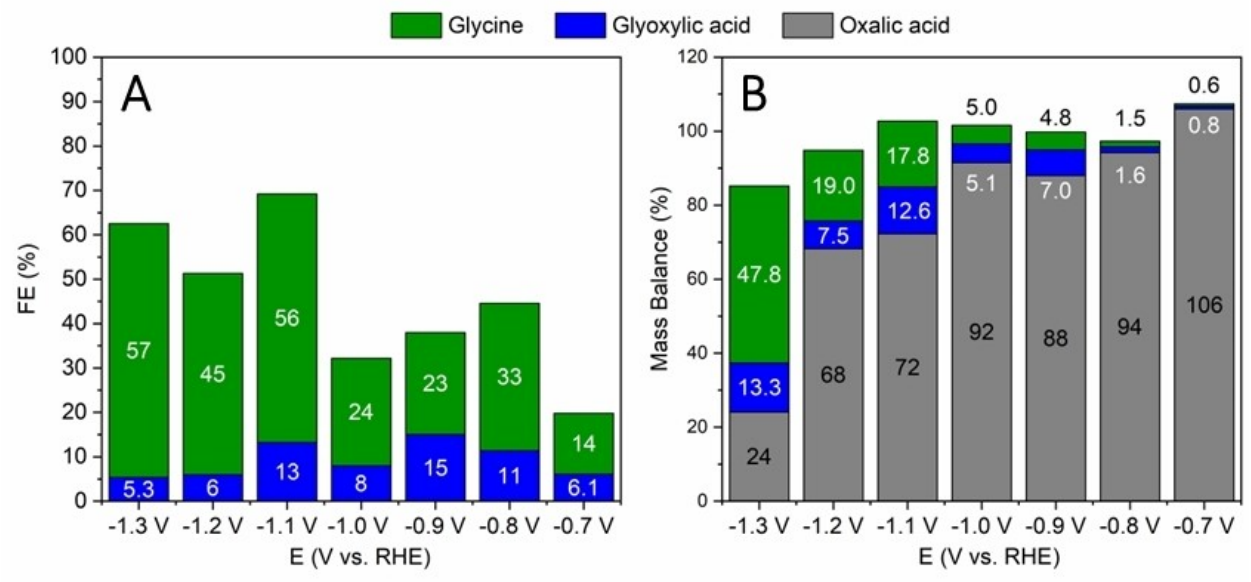

Figure 3. A) Faradaic efficiency and B) Product yield of the electroreductive amination of oxalic acid on $CuPb_{1ML}$ at different potentials.

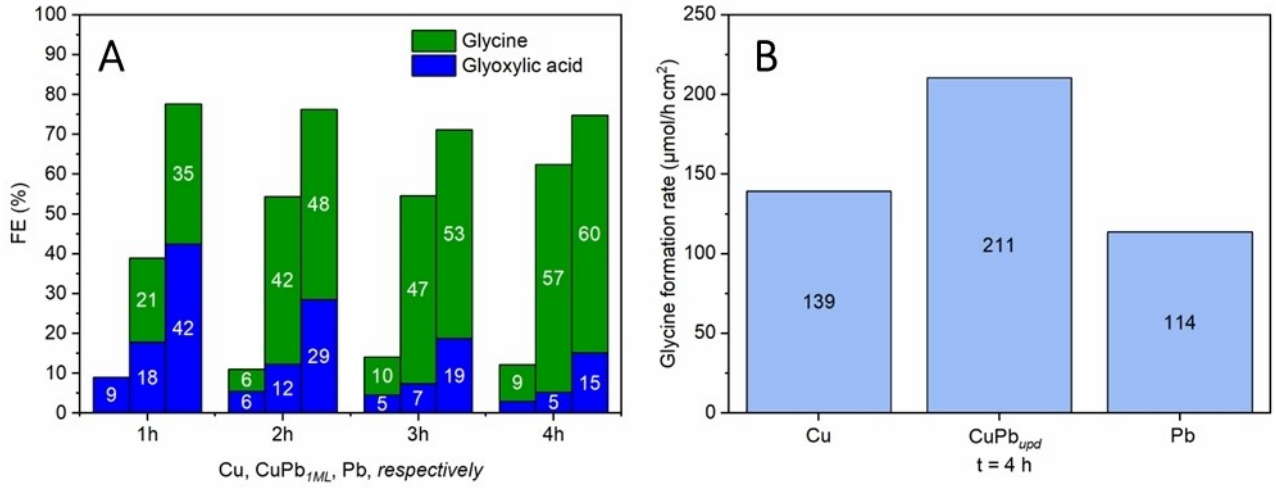

Figure 4. A) Total Faradaic efficiency for glycine and glyoxylic acid (cumulative) and B) Average glycine formation rate using Cu, $CuPb_{1ML}$, and Pb electrodes applying a potential of −1.3 V vs. RHE for 4 hours.

theless it opens the possibility to design catalysts which can be further optimized for glycine and other amino acids synthesis.

Mechanistic studies using in situ FTIR

The electroreductive amination of oxalic acid with hydroxylamine on the Cu, Pb and $CuPb_{1ML}$ electrodes are examined by using in situ FTIR. With this technique, we can gain insight into the mechanistic differences on each electrode, of which the spectra are shown in Figure 5. A summary of the most important bands is visible in Table 1. Reference spectra measured in 0.1 M H_2SO_4 are given in SI section 5. By monitoring several FTIR bands as a function of the applied potential, we can determine the production and consumption of the chemical species. The Pb electrode (Figure 5A), shows a small negative band at around 1700 cm^{-1} (C=O stretch from oxalic acid) at potentials more negative than −0.5 V vs RHE. As the potential decreases further, this band disappears, and two positive bands at 1745 cm^{-1} (C=O stretch) and 1238 cm^{-1} (C–O stretch) are formed, which are most likely associated with carbonyl and carboxylic acid groups, respectively.[35] These bands indicate the consumption of oxalic acid followed by formation of glyoxylic acid, which is converted to glyoxylic oxime upon reaction with hydroxylamine. At lower potentials, the relative intensity of these bands decrease, and small positive bands appears at 1415 cm^{-1} and 1326 cm^{-1} (Figure 5A, right inset). We assign these to the CH_2 scissoring and CH_2 waggle vibration of glycine, respectively. At −0.7 V vs. RHE, a positive band appears at 2345 cm^{-1}, associated with the C=O

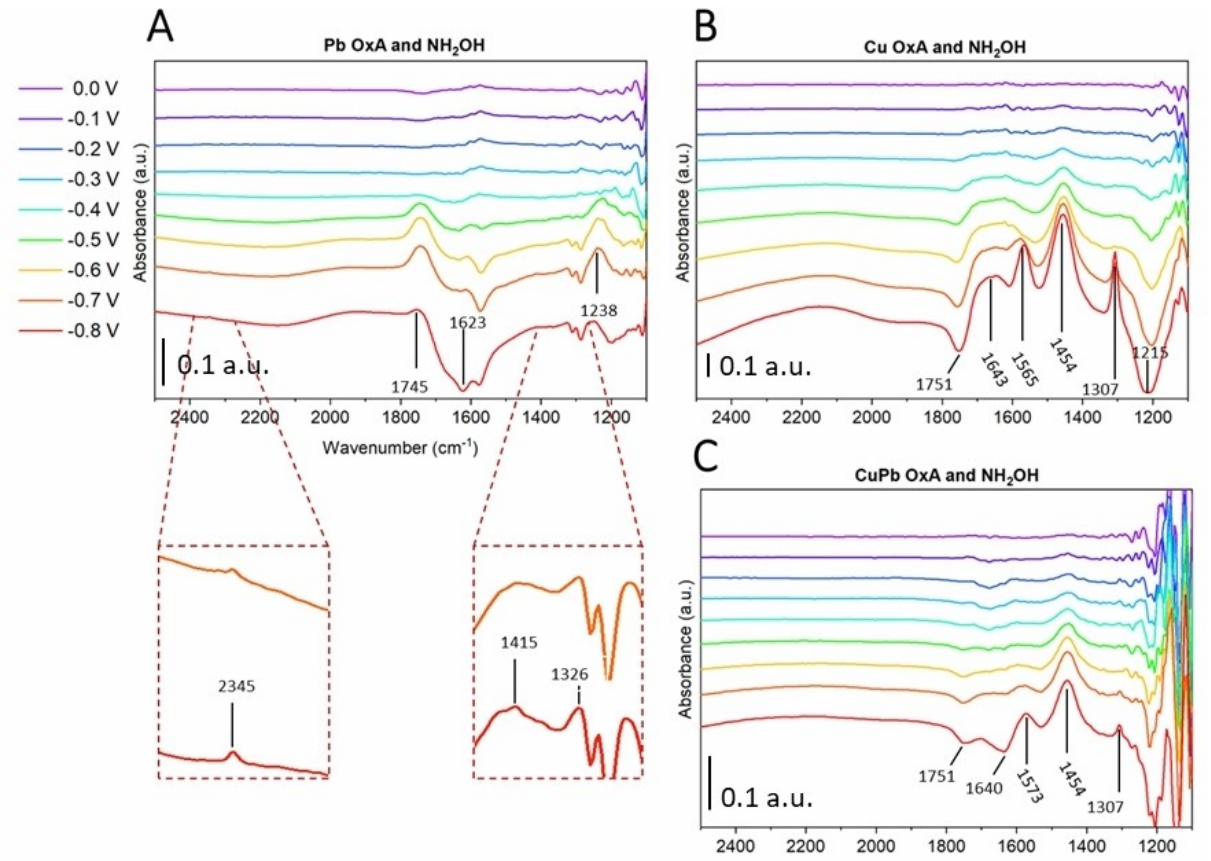

Figure 5. FTIR spectra at different potentials vs. RHE for the different electrode materials with 0.25 M oxalic acid and 0.25 M hydroxylamine in aqueous 0.1 M H_2SO_4. Spectra are shown for A) Pb, B) Cu and C) $CuPb_{1ML}$ electrodes. Reference spectra were taken at 0.0 V vs. RHE.

Table 1. FTIR absorption frequencies of different functional groups in glycine production on different electrode materials.[37]

Vibration (Compound)		Wavenumber (cm^{-1})			
Entry		Pure compound	Pb	Cu	$CuPb_{1ML}$
1	C═O str (Oxalic acid)	1750	1700	1751	1751
2	C–O str (Oxalic acid)	1232	–	1215	–
3	C═O str (glyoxylic acid/oxime)	1736/1722	1745	–	–
4	C–O str (glyoxylic acid/oxime)	1244/1221	1238	–	–
5	NH_2 sciss (glycine)	1630	–	1565	1573
6	NH_3^+ as def (glycine)	1634	–	1643	–
7	CH_2 sciss (glycine)	1443	1415	1454	1454
8	CH_2 wag (glycine)	1331	1326	1307	1307
9	C═O str (glycine)	1740	–	–	–
10	C–O str (glycine)		–	–	–
11	CO^-_2 s str (glycine)	1413	–	–	–
12	H–O–H b (water)	1644	1623	–	1640
13	O═C═O as str (CO_2)	2345	2345	–	–

stretching of CO_2 (Figure 5A, left inset[36]). This is likely due to the decarboxylation reaction of the oxime.[34] The appearance of a band at 1623 cm^{-1} at −0.8 V is related to O–H bending of water, reflecting the instability of the thin layer at more negative potentials due to hydrogen bubble formation.

On Cu and $CuPb_{1ML}$ electrodes (Figure 5B and C), from −0.4 V vs. RHE negative bands at 1751 cm^{-1} (C═O stretch) and 1215 cm^{-1} (C–O stretch) become visible. These bands reflect oxalic acid consumption. These electrodes also show large positive bands at potentials more negative than −0.5 V vs. RHE.

These bands appear at 1643 cm^{-1}, 1565/1573 cm^{-1}, 1454 cm^{-1} and 1307 cm^{-1}, which correspond to glycine production. Glycine undergoes significant shifts of IR vibration frequencies upon interaction with a copper surface.[37] The NH_2 scissoring vibration at 1630 cm^{-1} is blue-shifted to 1565/1573 cm^{-1}, the CH_2 scissoring vibration at 1432 cm^{-1} is red-shifted to 1454 cm^{-1} and the CH_2 waggle vibration is red-shifted from 1320 cm^{-1} to 1307 cm^{-1}. The band at 1643 cm^{-1} belongs to the NH_3^+ asymmetric deformation vibration. This vibration has not shifted, because when the glycine is protonated, it no longer strongly interacts with the copper surface.[37]

Importantly, we see no CO_2 bands, indicating that decarboxylation does not occur on the Cu and $CuPb_{1ML}$ electrodes at the measured potentials (minimum −0.8 V vs. RHE). In our bulk electrolysis results, the carbon balance only goes below 100% at potentials more negative than −1.2 V vs. RHE. Due to gas formation during the FTIR measurements, these potentials were not reached. Interestingly, the bands related to glyoxylic acid/oxime (1745 cm^{-1} and 1238 cm^{-1}) formation are absent. However, when performing the experiment with only oxalic acid as the substrate (Figure S8), the $CuPb_{1ML}$ electrode does show glyoxylic acid formation. This indicates that the latter is converted instantly to glycine in the presence of hydroxylamine.

Based on the *in situ* FTIR analysis, we assume that glycine has a weak interaction with the Pb surface, as there is only a faint glycine band. The well-defined bands on the Cu and $CuPb_{1ML}$ electrodes suggest a stronger interaction between the substrate and the electrode surface. This similarity was unexpected, given that the blue- and red-shifts that were observed typically indicate an interaction between glycine and the Cu surface. Since the SEM and XPS measurements of a freshly prepared $CuPb_{1ML}$ electrocatalyst reveal no Cu at the surface (*vide supra*, Figure S1), it would be unlikely that Cu would interact with the substrate. We therefore hypothesize that the $CuPb_{1ML}$ electrode undergoes changes related to the catalyst composition and structure under the reaction conditions, resulting in bare Cu exposed on the surface.

X-ray Photon-electron Spectroscopy & Scanning Electron Microscopy

We used SEM and XPS to examine the used $CuPb_{1ML}$ electrode to determine whether the composition and structure of the electrode changed during the reaction. For these measurements, 15 minutes of catalysis was performed at −1.1 V vs. RHE with 0.25 M oxalic acid and 0.25 M of hydroxylamine. SEM images of the $CuPb_{1ML}$ surface (Figure 6A, 6B, S13 A and S13B) show two types of microparticles on the surface, which are present in discrete regions on the electrode. Similarly, XPS shows the presence of two types of Pb species (Figure 6C and 6D), namely $PbSO_4$ (BE of 139.3 eV) and PbO (BE of 138.5 eV). $PbSO_4$ crystals are cubic[38] and the spherical particles are ascribed to PbO, as spherical PbO particles have been reported.[39] Therefore we attribute the particles in Figure 6A as $PbSO_4$ and those in Figure 6B as PbO. To quantify the morphological change of the $CuPb_{1ML}$ electrode the roughness factor was calculated before and after catalysis. Electrochemical Impedance Spectroscopy was used, which gave a roughness factor of 1.6 as compared to a pristine $CuPb_{1ML}$ catalyst (SI section 5.0).[40]

During electrolysis, the PbO monolayer on the surface is reduced to Pb, and then reorganizes to form microparticles. When the electrolysis is stopped, the microparticles re-oxidize upon contact with air. This yields either PbO, or $PbSO_4$ after complexing with SO_4^{2-} ions.[41] The formation of microparticles exposes bare Cu on the electrode surface during electrolysis explaining the interaction between Cu and the glycine as suggested by the *in situ* FTIR results. These findings were unexpected since partial coverage of Pb on the surface was expected to give low FE towards glycine, as HER (a facile reaction on Cu in acidic media) would then dominate the electrolysis. This counterintuitive finding prompted us to study the material further, to clarify the factors that cause HER inhibition.

Hochfilzer *et al.* found that in alkaline media during Pb UPD, the Pb atoms can incorporate into the Cu lattice (in addition to forming a monolayer[42]). This process is highly irreversible, and the Cu lattice can be restored only through (electro)polishing. We envisioned that in our system a similar process takes place. The lattice Pb atoms could suppress HER even if the Cu surface is not permanently or entirely covered with the Pb monolayer. To test this hypothesis, we synthesized a $CuPb_{doped}$ material via a standard UPD protocol, after which the electrode was held at 0.3 V vs. RHE until no more current flowed, indicating a full stripping of the monolayer. This yields a Cu electrocatalyst with a surface doping of Pb (see details in SI, section 7). This electrode was then analyzed via XPS and tested for the same amination reaction (Figure 7A and B, respectively).

The XPS spectra clearly showed the presence of lead as PbO by the Pb $4f_{7/2}$ at 138.4 eV (Figure 7A). The Pb $4f_{7/2}$ peak of the $CuPb_{doped}$ appears at a higher binding energy compared to the Pb $4f_{7/2}$ peak of the $CuPb_{1ML}$. This difference can be attributed to the formation of an alloy in the $CuPb_{doped}$ catalyst (see details in SI, section 8).

We then compared performance of this $CuPb_{doped}$ electrocatalyst to that of Cu and $CuPb_{1ML}$ by performing 4 hours of bulk electrolysis with 0.25 M oxalic acid and 0.25 M hydroxylamine using the standard conditions. The FE towards glycine (18%) and the activity (203 $\mu mol\,h^{-1}\,cm^{-2}$) of the doped electrocatalyst was between that of Cu and $CuPb_{1ML}$. In all electrocatalytic aspects the $CuPb_{doped}$ electrode outperformed Cu, even though the Pb content of this material was much lower than for the $CuPb_{1ML}$ electrocatalyst (~38 $ng\,cm^{-2}$ compared to 415 $ng\,cm^{-2}$ for $CuPb_{1ML}$, see SI section 8). Clearly, both the surface doping of Cu as well as the monolayer deposition play important roles in the inhibition of HER, as well as in promoting the conversion of oxalic acid and hydroxylamine to glycine synthesis. Figure 8 shows a schematic of the development of the electrode surface and the reaction pathway. After a short reaction time, the $CuPb_{1ML}$ electrocatalyst reorganizes to a surface with Pb microparticles which play a role as the active catalytic sites. However, the microparticle formation also

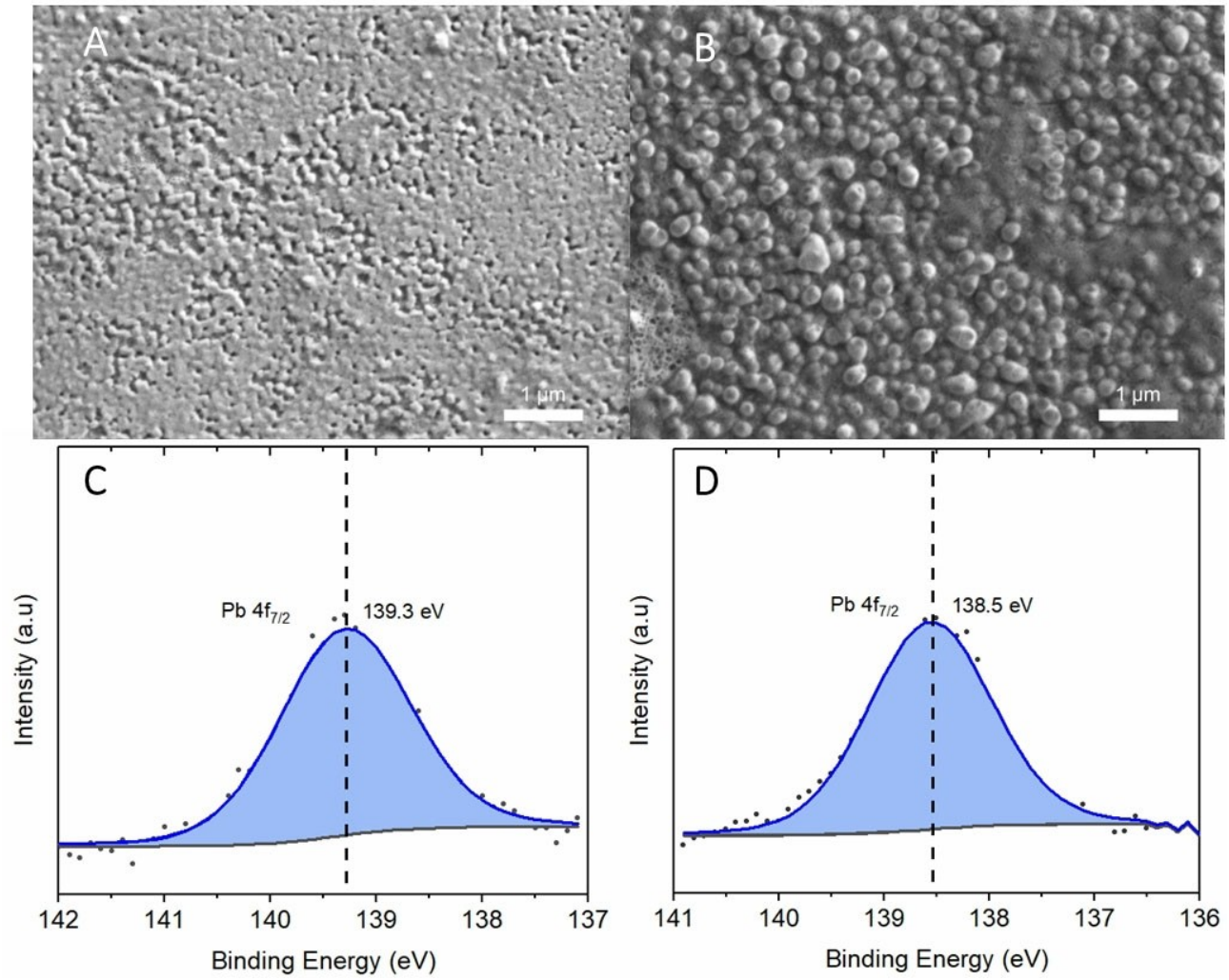

Figure 6. A, B) SEM imaging of a $CuPb_{1ML}$ electrode after catalysis on two different regions of the same electrode (25000x magnification, 2.00 kV accelerating voltage, ETD). C, D) XPS Pb 4 f scans of a $CuPb_{1ML}$ electrocatalyst after catalysis. Catalysis was performed at −1.1 V vs. RHE for 15 minutes with 0.25 M oxalic acid and 0.25 M hydroxylamine.

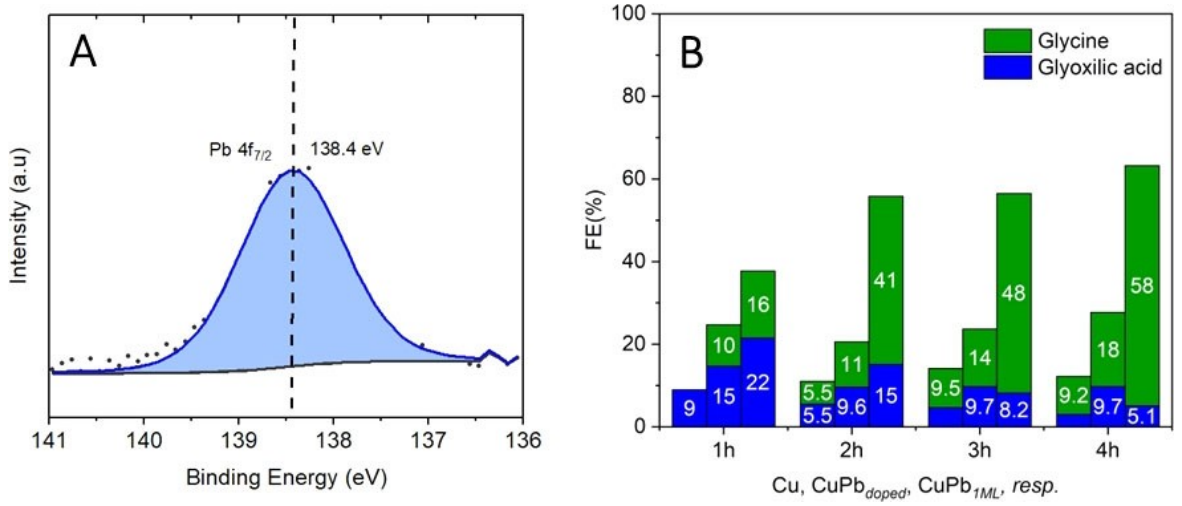

Figure 7. A) Pb 4 f XPS of the $CuPb_{doped}$ electrode. B) Electrolysis results of glycine synthesis for the $CuPb_{doped}$ electrode compared to Cu and $CuPb_{1ML}$ showing Faradaic efficiency over time with 0.25 M oxalic acid and 0.25 M hydroxylamine in 0.1 M H_2SO_4 in H_2O.

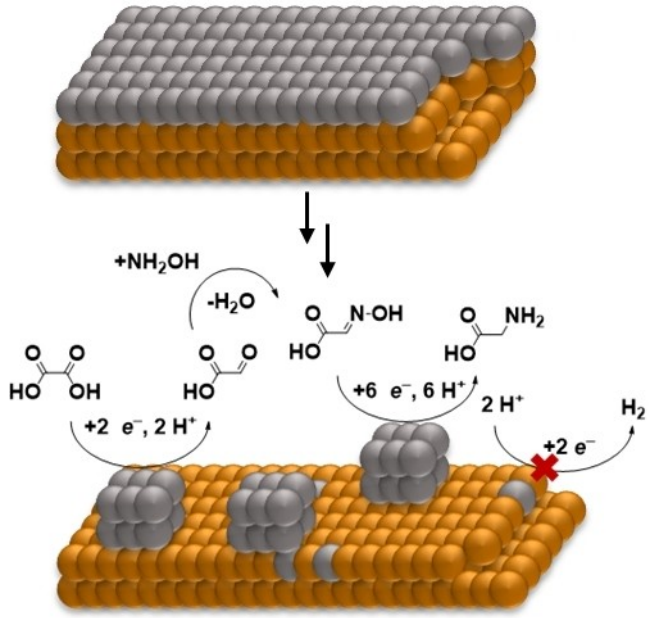

Figure 8. A schematic description of the $CuPb_{1ML}$ material restructuring and proposed mechanism of glycine synthesis on the $CuPb_{1ML}$ electrocatalyst. The pristine catalyst (Top) is shown to reorganize in microparticles, revealing the Pb doped Cu surface underneath (Bottom). Oxalic acid reduction, oxime formation and reduction is shown on the restructured catalyst, as well as the inhibition of HER.

exposes part of the copper surface. This copper is passivated for HER via surface doping, yielding a electrocatalyst where glycine production still dominates over the facile hydrogen evolution reaction.

Conclusions

In this research, we set out to design an electrode with a high overpotential to HER. Our goal was to achieve the performance of a Pb electrode, whilst using the minimum amount of Pb. We show that UPD is an effective method for making $CuPb_{1ML}$ electrocatalysts, and that such catalysts can facilitate the C–N bond formation during the electroreductive amination of oxalic acid to glycine. In comparison to a Pb and a Cu electrode, the $CuPb_{1ML}$ electrocatalyst does not behave identically to a Pb electrode in the production of glycine. A pure Pb electrode has a higher FE of 60% towards glycine production when compared to $CuPb_{1ML}$ (FE 57%), but the $CuPb_{1ML}$ electrode has higher catalytic activity (211 $\mu mol\,h^{-1}\,cm^{-2}$ vs. 114 $\mu mol\,h^{-1}\,cm^{-2}$). Additionally, $CuPb_{1ML}$ has a 9-fold higher FE towards glycine production when compared to pure Cu (9%), thanks to HER inhibition. By adding the Pb monolayer, the HER inhibiting effect of Pb is transposed upon the Cu electrode. During electrocatalysis, the Pb monolayer restructures, exposing some of the Cu surface, but this surface is less active in HER. This shows that there are two distinct pathways via which addition of Pb via UPD facilitates the glycine electrosynthesis, by surface modification through deposition of the Pb monolayer and by surface alloying of Pb in the top layer of the Cu surface. This $CuPb_{1ML}$ electrocatalyst opens exciting opportunities for alternative and more sustainable electrosynthetic procedures normally performed with traditional Pb electrodes.

Experimental section

Electrochemical measurements

All water used in this research was purified using a Milli-Q Millipore system with a total organic carbon content lower than 3 ppb and a resistivity higher than 18 MΩcm at room temperature. Prior to electrochemical experiments, all glassware was stored overnight in an aqueous 1 $g\,L^{-1}$ $KMnO_4$ (VWR chemicals, GPR RECTAPUR) and 0.5 M H_2SO_4 (Sigma-Aldrich, ACS reagent) solution. Before use, traces of $KMnO_4$ were removed from the glassware by rinsing at least three times with ultrapure water, followed by immersion in a dilute aqueous H_2SO_4/H_2O_2 (1:0.3 M) solution to oxidize organic and $KMnO_4$ residue. Afterwards, the glassware was boiled in fresh Milli-Q water three times before use.

All electrochemical experiments were performed at room temperature. For cyclic voltammetry (CV), a single compartment three-electrode electrochemical glass cell configuration was filled with 100 mL aqueous 0.1 M H_2SO_4 solution which was used as the supporting electrolyte. The electrolyte was prepared to have a final concentration of 0.25 M oxalic acid (Sigma-Aldrich, ACS reagent) and/or 0.25 M hydroxylamine sulfate (TCI chemicals, >98.0% purity). Glassy carbon (GC, MaTecK) and a HydroFlex Reversible Hydrogen Electrode (RHE, Gaskatel) were used as counter and reference electrodes (CE and RE), respectively. Before electrochemical measurements, the electrolyte was purged with N_2 gas (Linde Gas, 99.999%) for 15 minutes. The working electrodes (WE) used were either a Cu disc (Equilabrium, ø=5 mm) or Pb disc (Mateck, ø=5 mm, 99.99+%). The Cu electrode was electropolished for 3×10 seconds at 3.0 V vs. a Cu reference/counter electrode in an aqueous 66% (v/v%) H_3PO_4 solution before use. After electropolishing, the surface of Cu was characterized in a potential range between −0.25 V and 0.45 V vs. RHE in a deaerated 0.1 M NaOH (MaTecK, 99+%) solution (Figure S13). The Pb electrode was first mechanically polished with a 3.0 μm and a 1.0 μm diamond suspension (Buehler) on a MicroCloth polishing cloth (Buehler), after which it was electropolished in an aqueous 0.5 M H_2SO_4 solution at −1.8 V vs. Pt reference/counter for 500 seconds. A CV was made in the reaction mixture of 0.25 M oxalic acid and 0.25 M hydroxylamine sulfate in 0.1 M H_2SO_4 to ensure the removal of all PbOx species (Figure S14). The CuPb electrode containing 1 monolayer of Pb on Cu ($CuPb_{1ML}$) was synthesized as follows: the Cu electrode was prepared as previously described. but after characterizing the electrode surface, UPD[21] was performed at −0.1 V vs. RHE for 5 minutes in an aqueous electrolyte containing 0.01 M $HClO_4$ (Acros, ACS reagent) and 0.2 mM $Pb(ClO_4)_2$ (Sigma-Aldrich, 99.995%). The freshly prepared electrode is either used to confirm successful electrodeposition by performing a stripping CV, or it is used as the WE in the electrochemical procedures.

Bulk electrolysis

The preparative scale reactions were performed in a two-compartment electrochemical glass cell configuration divided by a Nafion-117 membrane (FuelCellstore). Each compartment was filled in with an aqueous 30 mL 0.1 M H_2SO_4 solution. 0.25 M oxalic acid and/or 0.25 M hydroxylamine sulfate were added to the catholyte compartment. The anolyte compartment contained a graphite (MaTecK, ø=6 mm, l=90 mm) CE. The catholyte compartment contained a

Hydroflex RHE (Gaskatel) and the WE, which was a Pb rod ($A_{surface}$ = 3.10 cm^2, MaTecK, 99.99 + %), a Cu wire ($A_{surface}$ = 0.498 cm^2, MaTecK, 99.99%), or a $CuPb_{1ML}$ wire ($A_{surface}$ = 3.76 cm^2, MaTecK, 99.99% Cu). The WEs were pretreated in the same fashion as for the CV experiments (*vide supra*). The solution was purged with N_2 gas (Linde Gas, 99.999%) for 15 minutes and subsequently kept under inert atmosphere by passing a constant N_2 stream over the solution. The electrolysis was performed at the desired potential while stirring at ~150 rpm in the catholyte compartment and with an unstirred anolyte compartment, using an Autolab Potentiostat (Metrohm M204). At each timepoint, three aliquots of 100 μL were taken from the reaction mixture for HPLC analysis (*vide infra*).

High Performance Liquid Chromatography analysis

Liquid products were detected using a high-performance liquid chromatography (HPLC) Agilent 1260 Infinity II system equipped with an Agilent Technologies Inc. Aminex HPX 87-H column (300×7.8 mm) and a RID and VWD detector. An isocratic chromatography method was used with an eluent of 5 mM H_2SO_4 in water and a column temperature of 65 °C.[43] Aliquots of the reaction mixture (100 μL) were diluted in 900 μL Milli-Q water containing 12.5 mM propionic acid as an internal standard, which has a well-known retention time under the employed conditions.[44] The product yield of oxalic acid, glyoxylic acid and glycolic acid was calculated by fitting the results on a predetermined regression line (Figure S15). Although glyoxylic acid was mostly converted to glyoxylic oxime in the reaction mixture, the column composition was such that the amount of glyoxylic oxime in the HPLC assay was negligible. A derivation method was employed to determine the amount of glycine, as described in literature (Scheme S1).[43] This was done by adding 200 μL of a 1 M KNO_2 solution to the samples after the initial HPLC assay, after which the samples were heated to 45 °C for 90 minutes in a convection oven. This procedure converted the glycine to glycolic acid. After subtraction of the previously determined concentration of glycolic acid the concentration of glycine in the reaction mixture was accurately determined (Figure S16).

In situ Fourier Transform Infra-Red Spectroscopy

In situ Fourier Transform Infra-Red (FTIR) spectroscopic measurements were performed to provide information about possible intermediates and products of the electrochemical reduction of oxalic acid and hydroxylamine. FTIR spectroscopic measurements were carried out in a Bruker Vertex 80-V IR spectrometer equipped with a liquid nitrogen cooled MCT detector. A Veemax III (PIKE Technologies) was positioned in the spectrometer, wherein a home-made three electrode spectroelectrochemical cell with a CaF_2 prism attached to the bottom was placed.[45] The cell was filled with approximately 20 mL of 0.25 M oxalic acid and/or 0.25 M hydroxylamine in 0.1 M H_2SO_4 electrolyte. Cu, Pb or $CuPb_{1ML}$ disks (MaTecK) were used as the WEs, whereas platinum and a home-made reversible hydrogen reference were used as the CE and RE, respectively. The WE was pressed against the CaF_2 prism to obtain a thin film configuration.[45] The cell was purged with argon for 15 minutes and subsequently kept under inert atmosphere. FTIR spectra were collected in a range of 4000–1000 cm^{-1} at a resolution of 8 cm^{-1} for 100 scans. Spectra were collected over a potential range in 0.1 V increments from 0.0 V to −1.1 V vs. RHE, or until hydrogen evolution deteriorated the quality of the data. The spectra are presented as absorbance, according to $A = -\log(R/R_0)$, where R and R_0 are the reflectance corresponding to the single beam spectra obtained at the sample and reference potentials, respectively. In these difference spectra, negative bands (pointing down) correspond to the species that were present on or near the electrode surface at the reference potential and that are "consumed" at the sample potential. Positive bands (pointing up) correspond to the formation of species at the sample potential. All the spectro-electrochemical experiments were performed at room temperature.

X-ray Photon-electron Spectroscopy & Scanning Electron Microscopy

The X-ray photoelectron spectroscopy data were acquired using a K-Alpha ultra-high vacuum X-ray photoelectron spectrometer manufactured by ThermoFisher Scientific. This instrument was equipped with a monochromatic aluminum anode (Kα = 1486.68 eV, 72 W) X-ray source featuring a spot size of 400 μm. The detection system comprised a 180° double focusing hemispherical analyzer with a 128-channel detector. During the measurements, the samples were subjected to a pass energy of 50 eV. The survey spectra were employed to ascertain the elemental composition of the samples. The elements detected were copper, lead, oxygen, and carbon. To assess the charging states of the elements of interest, we examined the core-level lines C 1 s, O 1 s, Cu 2p, Cu LMM, and Pb 4 f. Subsequently, the acquired spectra underwent processing using CasaXPS software. To calibrate the binding energy scale, the binding energy of C 1 s was set to 284.8 eV. For the XPS spectra analysis, a Shirley background was employed, and the curve fitting process utilized a Gaussian function GL (30) for Cu 2p and a Laurenzian asymmetric function LA (1.53, 243) for Pb 4 f. In particular, the Cu $2p_{3/2}$ spectra (RSF = 18.1471) were fitted by applying a peak area constraint for Cu^{2+} that was 1.36 times larger than the shake-up peak. An additional peak was introduced to account for the asymmetry of Cu^{2+}. The constraints for this additional peak were consistent, with the position set 1.4 eV higher than the main Cu^{2+} peak, and the full width at half maximum (FWHM) was adjusted to Cu^{2+} + 1.42. Similarly, the Pb 4 f spectra (RSF = 33.5294) were fitted by implementing a peak area constraint for Pb $4f_{7/2}$ that was 0.75 times larger than the Pb $4f_{5/2}$ peak area. A position constraint of 4.87 eV higher than Pb $4f_{7/2}$ was applied for the Pb $4f_{5/2}$ peak.

Scanning electron microscopy (SEM) analysis of the $CuPb_{1ML}$ electrodes were conducted on a ThermoFisher Apreo S electron microscope with an accelerating voltage of 2 kV and a 0.20 nA beam current. Everhart-Thornley and in-column detectors were used for imaging. Images were collected with a resolution of 1536×1024 and a pixel dwell time of 20–25 μs. SEM and XPS analysis was conducted on both a freshly prepared $CuPb_{ML}$ electrode and after catalysis at −1.1 V vs. RHE for 15 minutes with 0.1 M H_2SO_4, 0.25 M oxalic acid and 0.25 M hydroxylamine.

Supporting Information

The authors have cited additional references within the Supporting Information.[46–50]

Acknowledgements

The research was carried out under project numbers ECCM.TT.ECCM.008 and ECCM.TT.MVITU.005. Both research projects were carried out in the framework of the Electrochemical Conversion and Materials (ECCM) program and received funding from the Dutch Research Council (NWO).

Conflict of Interests

The authors declare no conflict of interest.

Data Availability Statement

The data that support the findings of this study are available from the corresponding author upon reasonable request.

Keywords: Catalysis · C–N bond formation · Lead monolayer · Organic electrosynthesis · Underpotential deposition

[1] J. Cabana, T. Alaan, G. W. Crabtree, M. C. Hatzell, K. Manthiram, D. A. Steingart, I. Zenyuk, F. Jiao, A. Vojvodic, J. Y. Yang, N. P. Balsara, K. A. Persson, D. J. Siegel, C. L. Haynes, J. Mauzeroll, M. Shen, B. J. Venton, N. Balke, J. Rodríguez-López, D. R. Rolison, R. Shahbazian-Yassar, V. Srinivasan, S. Chaudhuri, A. Couet, J. Hattrick-Simpers, *ACS Energy Lett.* **2022**, *7*, 368–374.
[2] Y. Yuan, A. Lei, *Nat. Commun.* **2020**, *11* (802), 1–3.
[3] J. E. Kim, J. H. Jang, K. M. Lee, M. Balamurugan, Y. I. Jo, M. Y. Lee, S. Choi, S. W. Im, K. T. Nam, *Angew. Chem. Int. Ed.* **2021**, *60*, 21943–21951.
[4] T. Fukushima, M. Yamauchi, *J. Appl. Electrochem.* **2021**, *51*, 99–106.
[5] N. Meng, J. Shao, H. Li, Y. Wang, X. Fu, C. Liu, Y. Yu, B. Zhang, *Nat. Commun.* **2022**, *13*, 1–8.
[6] Y. Wu, Z. Jiang, Z. Lin, Y. Liang, H. Wang, *Nat. Sustain.* **2021**, *4*, 725–730.
[7] D. Anastasiadou, B. Ligt, Y. He, R. C. J. van de Poll, J. F. M. Simons, M. C. Figueiredo, *Commun. Chem.* **2023**, *6* (199), 1–8.
[8] J. J. Roylance, K. S. Choi, *Green Chem.* **2016**, *18*, 5412–5417.
[9] C. Chen, X. Zhu, X. Wen, Y. Zhou, L. Zhou, H. Li, L. Tao, Q. Li, S. Du, T. Liu, D. Yan, C. Xie, Y. Zou, Y. Wang, R. Chen, J. Huo, Y. Li, J. Cheng, H. Su, X. Zhao, W. Cheng, Q. Liu, H. Lin, J. Luo, J. Chen, M. Dong, K. Cheng, C. Li, S. Wang, *Nat. Chem.* **2020**, *12*, 717–724.
[10] J. E. Kim, S. Choi, M. Balamurugan, J. H. Jang, K. T. Nam, *Trends Chem.* **2020**, *2*, 1004–1019.
[11] J. M. Barlow, J. W. Ziller, J. Y. Yang, *ACS Catal.* **2021**, *11*, 8155–8164.
[12] C. Gütz, V. Grimaudo, M. Holtkamp, M. Hartmer, J. Werra, L. Frensemeier, A. Kehl, U. Karst, P. Broekmann, S. R. Waldvogel, *ChemElectroChem* **2018**, *5*, 247–252.
[13] D. Strmcnik, P. P. Lopes, B. Genorio, V. R. Stamenkovic, N. M. Markovic, *Nano Energy* **2016**, *29*, 29–36.
[14] J. Seidler, A. Roth, L. Vieira, S. R. Waldvogel, *ACS Sustainable Chem. Eng.* **2023**, *11*, 390–398.
[15] S. Nitopi, E. Bertheussen, S. B. Scott, X. Liu, A. K. Engstfeld, S. Horch, B. Seger, I. E. L. Stephens, K. Chan, C. Hahn, J. K. Nørskov, T. F. Jaramillo, I. Chorkendorff, *Chem. Rev.* **2019**, *119*, 7610–7672.
[16] J. Y. Fang, J. L. Fan, S. B. Liu, S. P. Sun, Y. Y. Lou, *Mater.* **2023**, *16*, 4000.
[17] M. Jouny, J. J. Lv, T. Cheng, B. H. Ko, J. J. Zhu, W. A. Goddard, F. Jiao, *Nat. Chem.* **2019**, *11(119)*, 846–851.
[18] Y. Zhao, Y. Ding, W. Li, C. Liu, Y. Li, Z. Zhao, Y. Shan, F. Li, L. Sun, F. Li, *Nat. Commun.* **2023**, *14*, 1–12.
[19] J. Li, N. Kornienko, *Chem. Sci.* **2022**, *13*, 3957–3964.
[20] A. S. Sabir, E. Pervaiz, R. Khosa, U. Sohail, *RSC Adv.* **2023**, *13*, 4963–4993.
[21] E. Herrero, L. J. Buller, H. D. Abruña, *Chem. Rev.* **2001**, *101*, 1897–1930.
[22] L. Guo, S. Nayak, Y. Mao, N. Li, *Anal. Biochem.* **2021**, *635 (114447)*, 1–8.
[23] P. Sebastián-Pascual, M. Escudero-Escribano, *J. Electroanal. Chem.* **2021**, *896* (115446), 1–9.
[24] R. Vasilic, N. Vasiljevic, N. Dimitrov, *J. Electroanal. Chem.* **2005**, *580*, 203–212.
[25] K. Ahmadi, N. Dole, D. Wu, T. Salavati-Fard, L. C. Grabow, F. C. Robles Hernandez, S. R. Brankovic, *ACS Catal.* **2021**, *11*, 4650–4659.
[26] B. Vincent Crist, *Handbooks of Monochromatic XPS Spectra*, XPS International, Inc., **1999**.
[27] X. Zeng, S. Bruckenstein, *J. Electrochem. Soc.* **1999**, *146*, 2549–2554.
[28] The European Comission, *"Commission Regulation (EU) 2021/1317 of 9 August 2021 amending Regulation (EC) No 1881/2006 as regards maximum levels of lead in certain foodstuffs."*, can be found under https://eur-lex.europa.eu/legal-content/EN/TXT/?uri=celex%3A32021R1317, **2021** (accessed 12 June 2023).
[29] E. N. Codaro, J. R. Vilche, *Electrochim. Acta* **1997**, *42*, 549–555.
[30] C. Martin, H. Huser, K. Servat, K. B. Kokoh, *Electrochim. Acta* **2005**, *51*, 111–117.
[31] M. Gençten, K. B. Dönmez, Y. Şahin, K. Pekmez, E. Suvacı, *J. Solid State Electrochem.* **2014**, *18*, 2469–2479.
[32] D. Berndt, *Maintenance-Free Batteries: Based on Aqueous Electrolyte Lead-Acid, Nickel/Cadmium, Nickel/Metal Hydride: A Handbook of Battery Technology*. **2003**, p. 486.
[33] N. Farahbakhsh, S. Sanjabi, *J. Ind. Eng. Chem.* **2019**, *70*, 211–225.
[34] J. Xian, S. Li, H. Su, P. Liao, S. Wang, R. Xiang, Y. Zhang, Q. Liu, G. Li, *Angew. Chem. Int. Ed.* **2023**, *62*, e202306726.
[35] Sigma Aldrich, "IR Spectrum Table," can be found under https://www.sigmaaldrich.com/NL/en/technical-documents/technical-article/analytical-chemistry/photometry-and-reflectometry/ir-spectrum-table, (accessed on 17 June 2023).
[36] S. Chen, A. Chen, *J. Phys. Chem. C* **2019**, *123*, 23898–23906.
[37] S. M. Barlow, K. J. Kitching, S. Haq, N. V. Richardson, *Surf. Sci.* **1998**, *401*, 322–335.
[38] J. A. Bialacki, N. A. Hampson, K. Peters, A. K. Williams, *J. Appl. Electrochem.* **1983**, *13*, 103–104.
[39] C. G. Poll, D. J. Payne, *Electrochim. Acta* **2015**, *156*, 283–288.
[40] P. Connor, J. Schuch, B. Kaiser, W. Jaegermann, *Zeitschrift Fur Physikalische Chemie-Frankfurt* **2020**, *234*, 979–994.
[41] R. G. Barradas, D. S. Nadezhdin, *Can. J. Chem.* **1984**, *62* (3), 596–600.
[42] D. Hochfilzer, A. Tiwari, E. L. Clark, A. S. Bjørnlund, T. Maagaard, S. Horch, B. Seger, I. Chorkendorff, J. Kibsgaard, *Langmuir* **2022**, *38*, 1514–1521.
[43] D. Pleissner, R. Wimmer, N. T. Eriksen, *Anal. Chem.* **2011**, *83*, 175–181.
[44] "Guide to Aminex HPLC Colums." can be found under http://www.hplc.sk/pdf/Biorad/Guide_to_Aminex_HPLC_columns.pdf (accessed 24 August 2023).
[45] G. García, P. Rodríguez, V. Rosca, M. T. M. Koper, *Langmuir* **2009**, *25*, 13661–13666.
[46] T. P. Moffat, *J. Phys. Chem. B* **1998**, *102*, 10020–10026.
[47] B. C. Beard, *Surf. Sci. Spectra* **1993**, *2*, 97–103.
[48] P. Hale, S. Thurgate, P. Wilkie, *Surf. Interface Anal.* **2003**, *35*, 842–851.
[49] Y. A. Shao, Y. T. Chen, P. Y. Chen, *J. Electrochem. Soc.* **2019**, *166*, D221–D226.
[50] K. J. Klaas, E. P. Gallent, M. T. M. Koper, *J. Electroanal. Chem.* **2013**, *699*, 6–9.

Manuscript received: October 27, 2023
Revised manuscript received: November 24, 2023
Accepted manuscript online: December 12, 2023
Version of record online: January 25, 2024